4.1 ALONG-FRONTAL KINEMATIC AND MOISTURE VARIABILITY AND THE IMPACT ON CONVECTION INITIATION

Tammy M. Weckwerth[1]*, Hanne V. Murphey[2], Cyrille Flamant[3], Crystalyne R. Pettet[1] and Roger M. Wakimoto[2]

[1]National Center for Atmospheric Research**/Atmospheric Technology Division, Boulder, CO, USA
[2]Department of Atmospheric Sciences, University of California, Los Angeles, CA, USA
[3]Institut Pierre-Simon Laplace/Service d'Aéronomie, Centre National de la Recherche Scientifique, Paris, France

1. INTRODUCTION

The factors that influence the exact timing and location of newly-initiated deep moist convection are a hot research topic. Low-level convergence zones are often the precursors to convective development (e.g., Wilson and Shreiber 1986). Convection, however, usually does not develop in a uniform, solid band along the boundaries. In an effort to improve both scientific understanding and forecasting skill, potential causes for the along-boundary variability of convection initiation are examined.

Past work has shown that intersections between various low-level boundaries are more likely to be the locations for convective development. Such intersections include gust fronts with sea breeze fronts (e.g., Fankhauser et al. 1995), cold fronts with drylines (e.g., Schaefer 1986), and stationary boundaries with horizontal convective rolls (e.g., Wilson et al. 1995). Additionally past research has suggested that internal gravity waves may play a role in the development of new convection (e.g., Uccellini 1975).

This study will examine the detailed kinematics and thermodynamics at the intersections between an outflow boundary and internal gravity waves near the triple point between the outflow boundary and a dryline.

2. IHOP_2002

The International H_2O Project (IHOP_2002) was designed to sample the three-dimensional time-varying moisture field to better understand convective processes (Weckwerth et al. 2004). Numerous research and operational water vapor measuring systems and retrievals were operated in the U.S. Southern Great Plains from 13 May to 25 June 2002. This was done in combination with more traditional observations of wind and temperature. Convection initiation (CI) missions were designed to maximize observational overlap from multiple instruments to better understand the processes leading to the development of deep, moist convection. One particularly unique tool on the CI missions was a horizontal-pointing water vapor differential absorption lidar (DIAL; Leandre II) flown with an airborne Doppler radar (ELDORA) on-board a Naval Research Laboratory P-3 aircraft. In addition to the Leandre II, ELDORA and P-3 in situ measurements providing the moisture and kinematics along the boundaries, several other mobile datasets will be included in this study: a mobile radiometer; University of Wyoming King Air in situ instruments; Mobile Integrated Profiling System (MIPS); radiosondes and dropsondes. Although the ground-based sensors (i.e., S-Pol radar, mobile radars and mobile mesonets) were sampling the outflow boundary farther west than where convection initiated near the dryline, they are useful for illustrating the high-resolution boundary layer kinematics and thermodynamics.

Spectral analyses of numerous fields on 12 June 2002 identified internal gravity waves. The waves were interacting with two low-level boundaries (i.e., outflow boundary and dryline) prior to CI. The goal is to examine the moisture and kinematic variability associated with the waves, especially at the intersections between the waves and the boundaries. It is suspected that the waves may cause an along-boundary periodicity of moisture and vertical motion.

The combination of these high-temporal and -spatial resolution measurements will provide a detailed account of the interaction of various boundaries and waves and their impact on convective development.

3. 12 JUNE 2002 OVERVIEW

The GOES-11 satellite image in Fig. 1 shows a weak north-northeast/south-southwest oriented cold front, an east-west oriented outflow boundary with relatively cool, moist easterly air behind it toward the north and a northeast-southwest oriented dryline with warm, dry southerly flow toward the east. The winds were light and variable in the hot, dry air between the dryline and cold front. Note the linear cloud bands just north of the Oklahoma-Kansas border indicative of internal gravity waves. They are likely not cloud streets associated with horizontal convective rolls since they are oriented at a significant angle to the low-level wind direction.

The surface winds clearly define a subsynoptic low centered on the eastern edge of the Oklahoma Panhandle. The dryline is quite pronounced with a well-defined cloud line and significant moisture contrast across the zone.

As will be shown with the radar data in the following section, deep convection develops near the triple point between the outflow and dryline and south-westward along the dryline by 2055 UTC.

* *Corresponding author address*: Tammy M. Weckwerth, NCAR, P.O. Box 3000, Boulder, CO 80307-3000, USA. E-mail: tammy@ucar.edu

** NCAR is sponsored by the National Science Foundation.

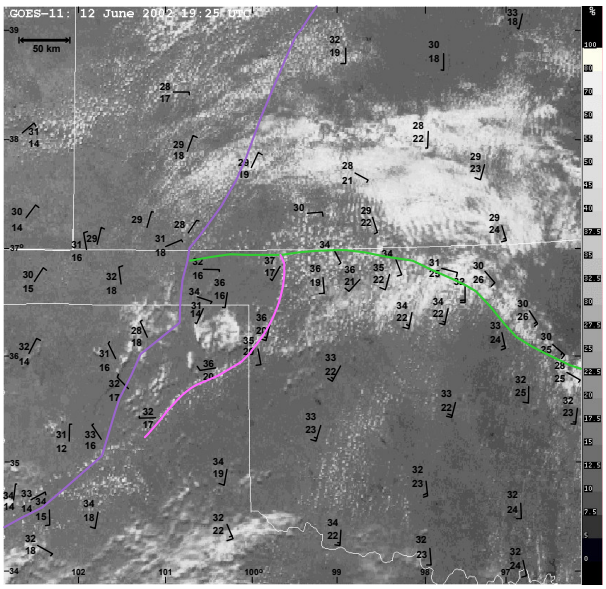

Fig. 1. Visible satellite image from 1925 UTC 12 June 2002. Purple line to the west indicates cold front, magenta line is the dryline and green line is an outflow boundary. Select surface stations are shown with temperature and dewpoint temperature (ºC) indicated. Half barb is 2.5 m s^{-1} and full barb is 5 m s^{-1}.

4. BOUNDARIES

The reflectivity composites in Figs. 2 and 3 show the reflectivity signature associated with the triple point between the three air masses: i) post-gust front air north of the outflow boundary, ii) warm, moist air east of the dryline and iii) hot, dry air west of the dryline. The fine lines associated with these boundaries are apparent. The cold front is more diffuse and less defined but still apparent. The north-south bands of enhanced reflectivity, perhaps indicative of internal gravity wave updrafts, are visible east of the triple point. Convection initiation occurred just before 2100 UTC, apparent by the small echo just southeast of the triple point between the outflow boundary and dryline (Fig. 3).

5. DROPSONDES

Two dropsonde legs normal to the outflow boundary were obtained. The drop locations are shown in Figs. 2 and 3. The second dropsonde leg commenced approximately 90 min after the first (2047:38-2111:38) and the composite is shown in Fig. 4. While the air mass behind the outflow boundary warmed and moistened since the first leg, the low-level winds remained easterly. The CBL depth remained nearly the same (~760 mb). The region west of the dryline was dry and hot with a deeper boundary layer (~670 mb) and southwesterly flow. This dropsonde leg included one drop that was south of the outflow boundary and just east of the dryline that was fortuitously dropped quite near the time

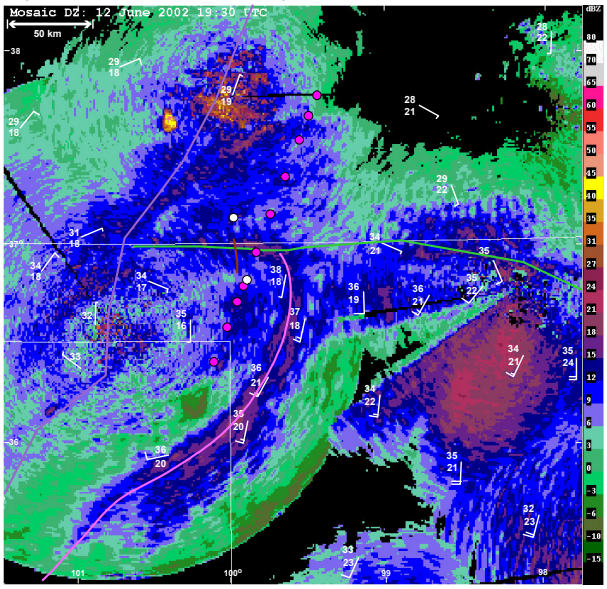

Fig. 2. Radar reflectivity composite at 1930 UTC 12 June 2002. Dots indicate locations of first leg dropsonde releases. Surface stations and boundaries are as in Fig. 1.

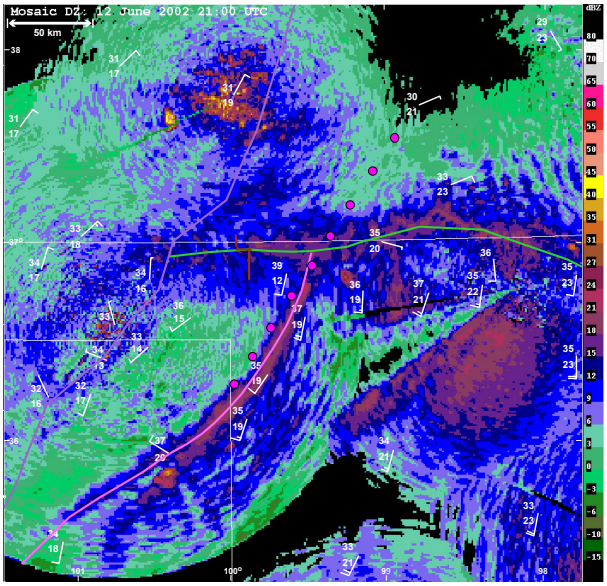

Fig. 3. Radar reflectivity composite at 2100 UTC 12 June 2002 just after the time of convection initiation near the triple point. Dots indicate locations of second leg dropsonde releases. Surface stations and boundaries are as in Fig. 1.

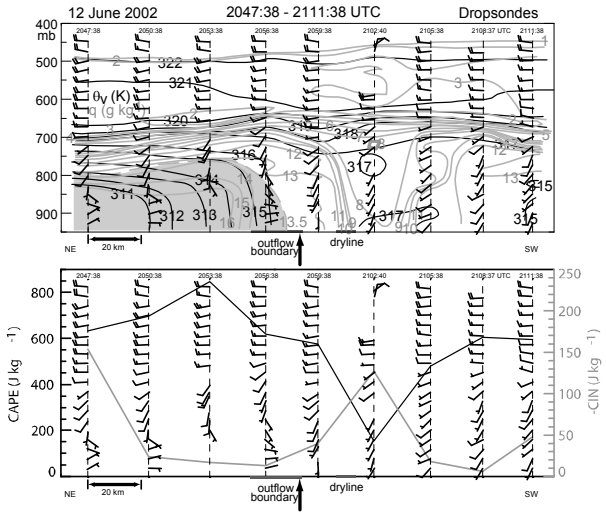

Fig. 4. Composite dropsonde analyses from 2047-2112 on 12 June 2002 with virtual potential temperature (K) in black and mixing ratios (g kg^{-1}) in gray in the top panel. Horizontal wind measured by each sonde is shown with the same format as in Fig. 1. The locations of the outflow boundary and dryline are indicated with gray line segments and CI location is shown by an arrow at the bottom of each panel. Bottom panel shows CAPE (J kg^{-1}; black line) and CIN (J kg^{-1}; gray line).

and location of convection initiation. This air mass exhibited the deepest moist layer of these two dropsonde composites. The Convective Available Potential Energy/Convective Inhibition (CAPE/CIN) composite for these dropsonde data shows that the most unstable region, with the lowest CIN and highest CAPE, occurs near and just north of the leading edge of the outflow boundary (Fig. 4; bottom). Interestingly the dropsonde in the CI airmass did not exhibit the most instability of the dropsonde composite.

6. ELDORA and LEANDRE II

The NRL P-3 aircraft housed two unique and complementary remote sensing instruments: NCAR's ELDORA airborne Doppler radar (e.g., Hildebrand et al. 1996) and CNRS's Leandre II airborne water vapor differential absorption lidar (e.g., Bruneau et al. 2001). Leandre II was flown in a horizontal-pointing mode for this mission to obtain a narrow swath of water vapor mixing ratio measurements. While ELDORA provided reflectivity and Doppler velocity measurements within the clear-air and precipitation regions, Leandre II provided clear-air water vapor measurements within the immediate vicinity of the outflow boundary.

The ELDORA and Leandre II data were processed

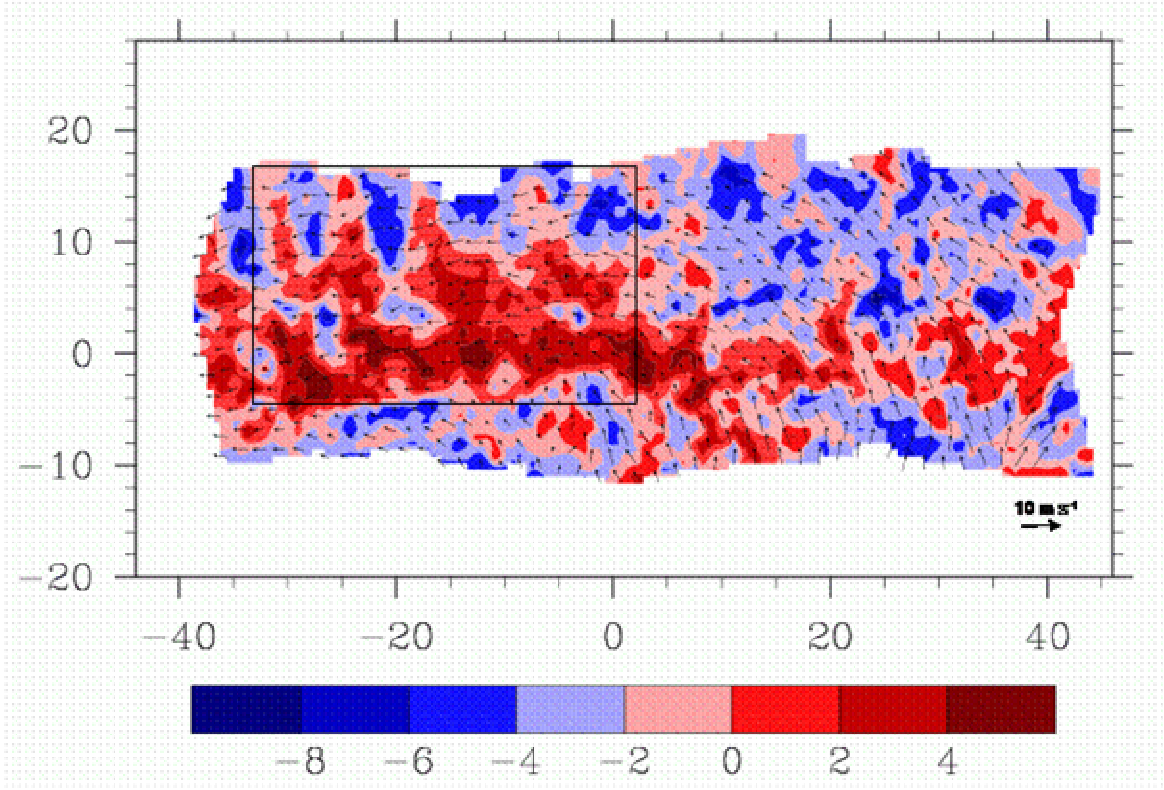

Fig. 5. ELDORA reflectivity and dual-Doppler-derived winds at 600 m AGL 2009-2021 UTC 12 June 2002. Black box indicates region to be shown in Fig. 6.

and combined as in Murphey et al. (2005). The ELDORA reflectivity field and derived wind field are shown in Fig. 5. Since the triple point indicates the boundaries between three distinct air masses with different wind fields, one might expect the cyclonic circulation to be centered on the triple point. There is, however, a displacement between the cyclonic circulation center and the triple point. The banded structure north of the outflow boundary is apparent. The Leandre II data provide only a sliver of measurements out the right side of the aircraft but are instructive in gleaning more information about the moisture field.

The Leandre II data within the box of Fig. 5 are shown in Fig. 6, along with the vertical vorticity field which clearly illustrates the banded structure associated with the waves. It is suspected that the vertical vorticity field illustrates the waves due to tilting of the westward-directed environmental shear vector north of the outflow. Note the strong correspondence between the vertical vorticity minima and the mixing-ratio maxima suggesting that the waves act to concentrate the moisture into the updraft branches. This will be examined further with other time periods.

7. SUMMARY

The multiple datasets collected on 12 June 2002 allow for the examination of various boundaries and wave interactions and their influence on convection initiation. The boundaries and waves were well-sampled by ELDORA, Leandre II and dropsondes. Additional supporting information from the diverse array of IHOP_2002 instrumentation will be added.

ACKNOWLEDGMENTS

This research is supported through the NCAR/USWRP program, NSF grant number ATM-012048 and NSF grant number ATM-0208651.

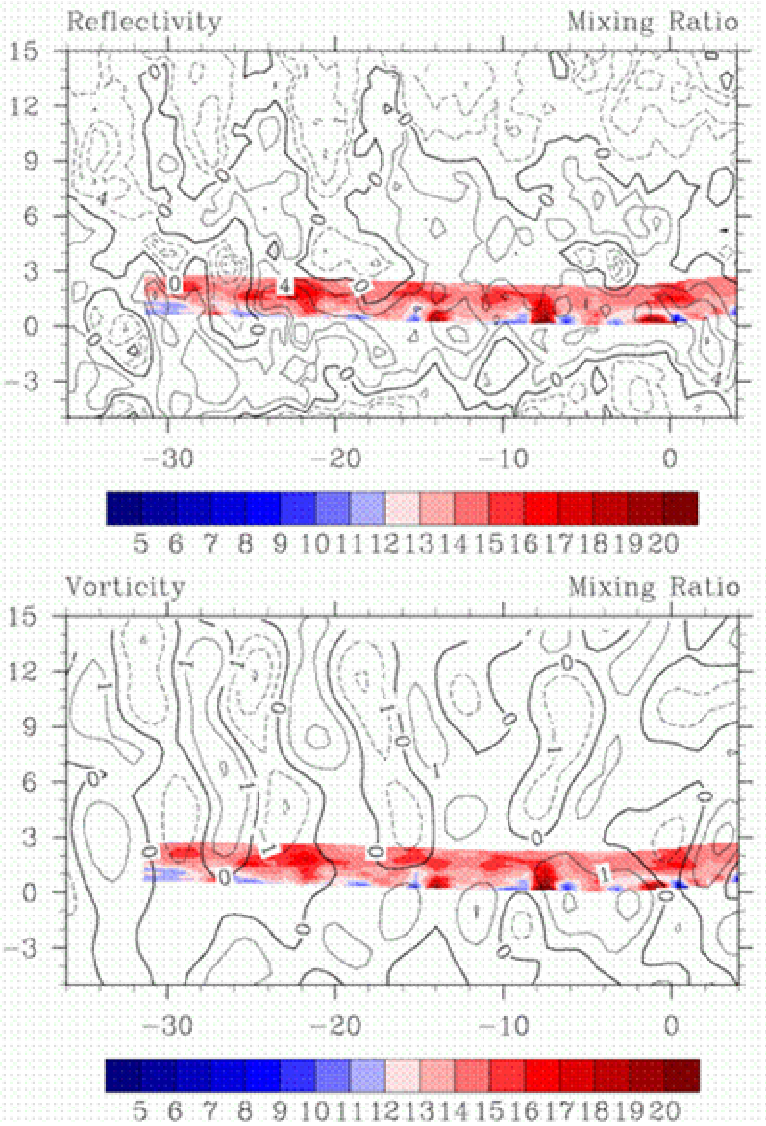

Fig. 6. Leandre II mixing ratio (g kg^{-1}) and ELDORA reflectivity (top; dBZ$_e$) and vertical vorticity (bottom; x 10^{-3} s^{-1}) at 600 m AGL 2009-2021 UTC 12 June 2002 within the box of Fig. 5.

8. REFERENCES

Bruneau, D., P. Quaglia, C. Flamant, M. Meissonier, and J. Pelon, 2001: Airborne lidar LEANDRE II for water-vapor profiling in the troposphere. *Appl. Opt*., **40**, 3450-3475.

Fankhauser, J. C., N. A. Crook, J. Tuttle, L. J. Miller, and C. G. Wade, 1995: Initiation of deep convection along boundary layer convergence lines in a semitropical environment. *Mon. Wea. Rev*., **123**, 291-313.

Hildebrand, P. H., and Coauthors, 1996: The ELDORA/ASTRAIA airborne Doppler weather radar: High-resolution observations for TOGA COARE. *Bull. Amer. Meteor. Soc*., **77**, 213-232.

Murphey, H., R. M. Wakimoto, C. Flamant, and D. E. Kingsmill, 2005: Dryline on 19 June 2002 during IHOP. Part I: Airborne Doppler and Leandre II analyses of the thin line structure and convection initiation. *Mon. Wea. Rev. IHOP_2002 Special Issue*, accepted.

Schaefer, J. T., 1986: The dryline. *Mesoscale Meteorology and Forecasting,* P. S. Ray, Ed., Amer. Meteor. Soc., 549-572.

Uccellini, L. W., 1975: A case study of apparent gravity wave initiation of severe convective storms. *Mon. Wea. Rev*., **103**, 497-513.

Weckwerth, T. M., D. B. Parsons, S. E. Koch, J. A. Moore, M. A. LeMone, B. B. Demoz, C. Flamant, B. Geerts, J. Wang and W. F. Feltz, 2004: An overview of the International H_2O Project (IHOP_2002) and some preliminary highlights. *Bull. Amer. Meteor. Soc*., **85**, 253-277.

Wilson, J. W., G. B. Foote, N. A. Crook, J. C. Fankhauser, C. G. Wade, J. D. Tuttle, C. K. Mueller, and S. K. Krueger, 1992: The role of boundary-layer convergence zones and horizontal rolls in the initiation of thunderstorms: A case study. *Mon. Wea. Rev*., **120**, 1785-1815.

Wilson, J. W., and W. E. Schreiber, 1986: Initiation of convective storms at radar-observed boundary-layer convergence lines. *Mon. Wea. Rev*., **114**, 2516-1536.